Hindawi
International Journal of Aerospace Engineering
Volume 2020, Article ID 1902053, 8 pages
https://doi.org/10.1155/2020/1902053

Research Article

Pitot Tube-Based Icing Detection: Effect of Ice Blocking on Pressure

Xianglian Lv,[1] Jie Guan,[1] Shengkun Wang,[1] Haiyang Zhang,[2] Shijie Xue,[1] Qi Tang,[1] and Yang He[1]

[1]*Key Laboratory of Micro/Nano Systems for Aerospace, Ministry of Education and Shaanxi Key Provincial Laboratory of Micro and Nano Electromechanical Systems, Northwestern Polytechnical University, Xi'an 710072, China*
[2]*China Aerodynamics Research and Development Center, Mian Yang 621000, China*

Correspondence should be addressed to Yang He; heyang@nwpu.edu.cn

Received 5 December 2019; Revised 24 February 2020; Accepted 9 May 2020; Published 13 August 2020

Academic Editor: Maj D. Mirmirani

This study aims at addressing a problem on icing detection for Unmanned Aerial Vehicle (UAV for short) because traditional icing detection methods are costly and bulky. Toward this end, a pitot-based icing detection method is proposed, and the effect of different types of icing blocking on pressure is firstly reported. An icing detection system based on the pitot tube is designed and fabricated. Icing wind tunnel results indicate that if the pitot tube is blocked by glaze ice, then the total pressure of the pitot tube decreases gradually and remains unchanged and less than static pressure. However, if the pitot tube is blocked by rime ice, then the total pressure drops to the same level as the static pressure. If the pitot tube is blocked by non-ice organic materials, then the total pressure suddenly drops to the same level as the static pressure and remains unchanged. Furthermore, if the pitot tube contacts the water droplets but does not freeze, the total pressure output value fluctuates slightly. The effect of icing on pressure is caused by differences in ice microstructure, temperature, and flow velocity. At the same time, the proposed method offers a facile and low-cost approach for UAV icing detection.

1. Introduction

UAVs are small, lightweight, and flexible in flight; furthermore, accomplish tasks that are difficult for ordinary aircraft while consuming relatively low energy. At present, UAVs are widely used in cold regions and highland areas for cruising, topographic mapping, patrolling border areas, surveying plateau areas, and inspecting transmission lines [1]. However, when working in cold regions and plateaus, UAVs encounter freezing weather conditions, which result in icing.

Aircraft icing, especially ice on the surface of the wing, seriously affects flight safety. Ice accretion on airfoils can cause severe damage to aircraft not only by increasing its weight but also by deteriorating aerodynamic capabilities and decreasing available lift force, thus affecting stability and safe operation [2–6]. Therefore, detecting icing on UAVs is particularly important [7].

Currently, the commonly used methods for detecting icing are optical, thermal, electrical, and mechanical methods [8–10], which are based on sensors. Such sensors are placed on ice-prone areas to sense the shape and thickness of the ice. However, these icing detection methods are costly, bulky, and relatively mature on large aircraft. These common techniques, when applied to UAVs, not only increase weight and volume but also greatly increase the cost. Thus, a facile and low-cost icing detection method is necessary for UAV safety.

Icing detection based on the pitot tube is a possible solution due to its ease of use and low cost. As a necessary component for UAVs to detect airspeed, the pitot tube is widely used because of its simple structure, reliable data, and resistance to destruction [11]. To detect ice accumulation on an aircraft wing, the pitot tube should be installed on the wing instead of the nose. After the total and static pressure holes of the pitot tube are blocked, the output value changes

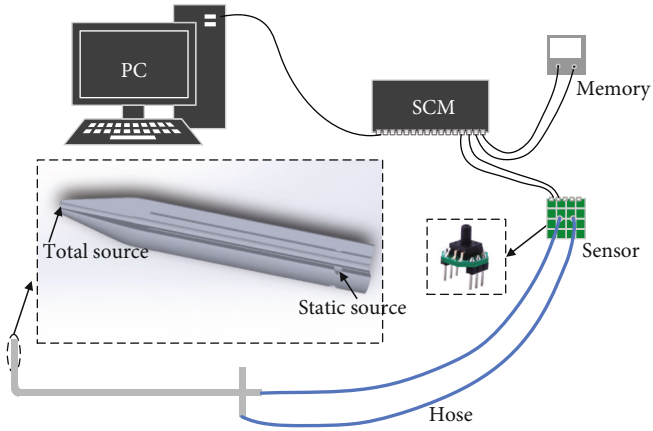

Figure 1: Icing detection system based on the air pressure measurement of the pitot tube.

accordingly. Therefore, the icing blocking characteristics of the pitot tube can be used as a basis for UAV icing detection. The influence of different ice types and materials on the pressure of the pitot tube is the basis of its application. However, the effect of icing on pressure and the corresponding mechanism remains unclear.

Therefore, this study investigates an icing detection method based on the pitot tube and the effect of icing on pressure in detail. An icing detection system based on the pitot tube is designed and fabricated. Then, experiments that include the blocking of ice, non-ice organic materials, and water spray are designed and implemented. Findings show that glaze ice, rime ice, non-ice organic materials, and water lead to different results in total and static pressure, which can be used for icing detection. Corresponding models for glaze and rime ice are established to elucidate the effects of such materials on pressure.

The remainder of this paper is structured as follows: Section 2 introduces the experimental design and experimental preparation. Section 3 discusses and analyzes the experimental results. Section 4 presents the conclusions.

2. Experiments

The icing detection system based on the pitot tube is first designed and fabricated. The system includes an L-shaped pitot tube, an air pressure sensor, a CPU, a hose, and other components, as shown in Figure 1.

This system selects a common L-shaped pitot tube, which has a diameter of 5 mm and a length of 35 mm. It consists of two concentric tubes, namely, the inner and outer tubes. The inner tube refers to the total pressure tube; the total pressure hole is situated at the top of the pitot tube. The outer tube is a static pressure tube; the static pressure hole is located on the side wall of the pitot tube [12]. The two nozzles are individually introduced into the air pressure sensor through the hose. After processing by the CPU, the total and static pressure data can be measured. Typically, the dynamic pressure calculated by the pitot tube is used to measure aircraft speed. However, this study only records the total and static pressure data of the pitot tube and bypasses differential pressure processing.

Table 1: Sensor parameters.

Voltage	0.5 V	1.5 V	2.5 V	3.5 V	4.5 V
Air pressure	−40 kPa	−20 kPa	0 kPa	20 kPa	40 kPa

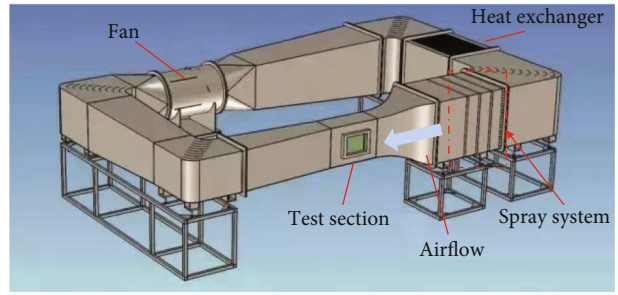

Figure 2: Icing wind tunnel (0.3 m × 0.2 m).

In measuring the total and static data, the selection of the air pressure sensor should not only consider the range but also the shape of the hose interface. The final selected sensor type is XGZP6847040KPGPN, and the measurement type is gauge pressure. Table 1 provides the parameters of this sensor.

In the entire hardware system for air pressure detection, the CPU requires a digital signal output from the AD converter and transmits such signal to the computer through a serial port for processing. The main control circuit used in the system is an Arduino UNO development board of ATmega328 MCU, which has 14 digital I/O pins, six analog signal input pins, and a 32 KB flash memory.

The system can collect the total and static pressure values of the pitot tube in real-time and transmit it to the computer through serial port communication to draw the total and static pressure curves and complete the measurement and detection of the air pressure data in the experiment.

To determine the characteristics of output data after the pitot tube is blocked by ice, the system performs numerous experiments in the ice wind tunnel environment. As shown in Figure 2, the 0.3 m × 0.2 m ice wind tunnel includes a stable, contraction, test, and fan section; a heat exchanger; and a refrigeration and spray system.

The experiments are mainly divided into three parts, namely, ice blocking, non-ice organic material blocking, and water spray experiments.

3. Results and Discussions

3.1. Ice Blocking Experiment. The ice blocking experiment is divided into two groups, namely, A and B. Table 2 displays the parameters for experiment A, such as temperature, wind speed, mean volume diameter (MVD), and liquid water content (LWC). Temperature and wind speed are selected from common icing conditions due to the limitations of the ice tunnel equipment. MVD and LWC are selected from the airworthiness standard CCAR/FAR-25 appendix. The pitot tube is mounted on the hole at the side wall of the test section facing the incoming flow direction. Figure 3 depicts the installation location.

Figure 4 displays the experimental results of group A. The figure shows that when the pitot tube detection system is stationary, the total and static pressure output by the system are nearly the same, and the pressure difference is nearly negligible. When the pitot tube is placed in the ice wind tunnel, the total pressure rises rapidly, whereas static pressure remains nearly unchanged. The spray system is turned on at point B. At this time, the water droplets remain in an unfrozen state and hits the pitot tube such that the total pressure is in a fluctuating state. After point C, the pitot tube begins to freeze, ice accumulates, and the total pressure decreases. After point D, the pitot tube is completely blocked by rime ice, and the output value of the total pressure hole drops to that of static pressure.

Table 3 provides the parameters of experiment B, and Figure 5 displays the results. It shows that the total static pressure and data for static pressure of the system before icing are similar to those of experiment A from point O to C. After point C, the pitot tube begins to freeze, ice accumulates, and total pressure decreases. After point D, the pitot tube is completely blocked by glaze ice, and the total pressure output value continues to decrease, finally, it is less than static pressure and remain stable.

It is noticeable that the photos of rime ice in Figure 6 and glaze ice in Figure 7 are taken by traditional camera after the stop of the experiment and remove of the baffle of ice wind tunnel. Unfortunately, the photos of the ice accretion process near the total pressure hole of the pitot tube could not be afforded due to experiment condition constraints. The test section of the ice wind tunnel is narrow and sealed by a baffle during the experiment, thus it is difficult to place a camera in the ice wind tunnel. Besides professional camera which could record the icing process near the total pressure hole with diameter 1-2 mm is lacked.

3.2. Non-Ice Organic Material Blocking Experiment. In actual flight, the pitot tube may be blocked by non-ice organic materials, such as insects. Thus, a non-ice organic material blocking experiment is designed and implemented. A rubber sleeve which is a type of organic material is used for testing as an alternative because insects are difficult to manipulate, as shown in Figure 8. Table 4 provides the parameters for experiment C, and Figure 9 demonstrates the experimental results of group C. The figure shows that when the pitot tube is blocked by the rubber sleeve, the total pressure first rises abruptly and then immediately decreases to the same level as the static pressure. This phenomenon is clearly different from the blockage of the pitot tube by ice.

3.3. Water Spray Experiment. This part of the experiment is also conducted in the icing wind tunnel and divided into

Table 2: Parameters of ice blocking experiment A.

Experimental conditions	Mean volume diameter	Liquid water content	Temperature	Wind speed
Data	22 μm	0.715 g/m^3	−5°C	15.6 m/s

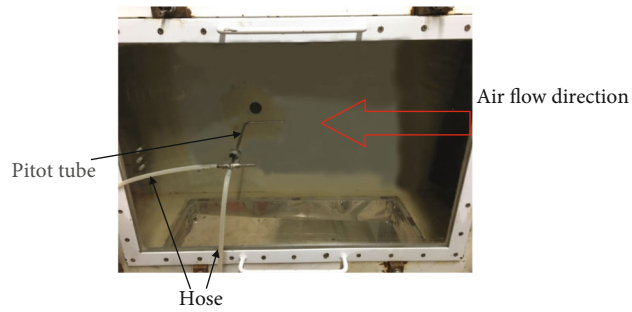

Figure 3: Schematic of the pitot tube installation in the test section.

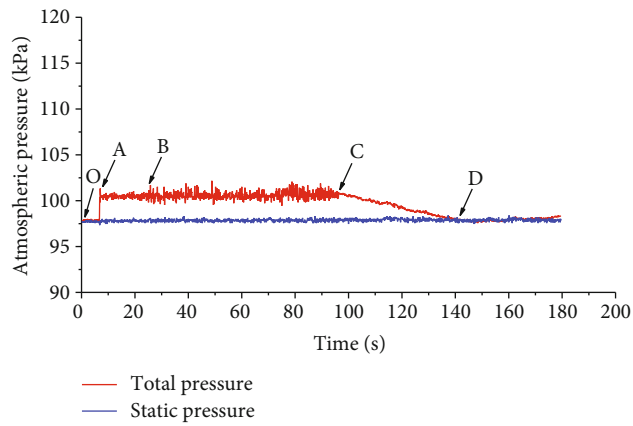

Figure 4: Total and static pressure outputs of the pitot tube after blocking by rime ice. O–A: the entire air pressure detection system is stationary. A–B: the L-shaped pitot tube is placed into the ice wind tunnel at point A, such that the total pressure hole is facing the incoming wind direction. B–C: the spray system is turned on at point B. C–D: after point C, the pitot tube is in an icy state, ice accumulates, and the icing state is rime ice (as shown in Figure 5). After point D, the ice shape is basically stable.

Table 3: Parameters of ice blocking experiment B.

Experimental conditions	Mean volume diameter	Liquid water content	Temperature	Wind speed
Data	22 μm	0.715 g/m^3	−5°C	7.9 m/s

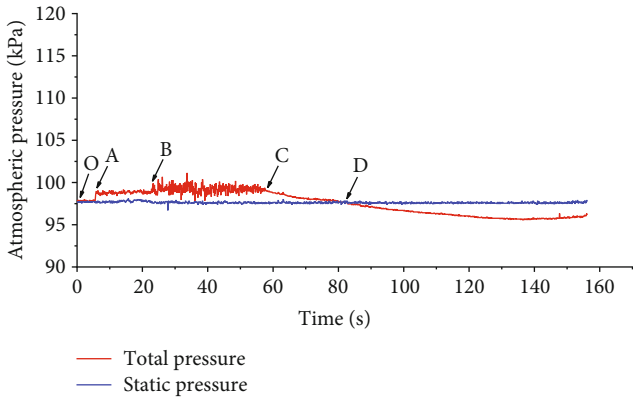

Figure 5: Total and static pressure outputs of the pitot tube after blocking by glaze ice. O–A: the entire air pressure detection system is stationary. A–B: the L-shaped pitot tube is placed into the ice wind tunnel at point A such that the total pressure hole is facing the incoming wind direction. B–C: the spray system is turned on at point B. C–D: after point C, the pitot tube is in an icy state, and icing state is glaze ice (as shown in Figure 7). After point D, the pitot tube is completely blocked by glaze ice.

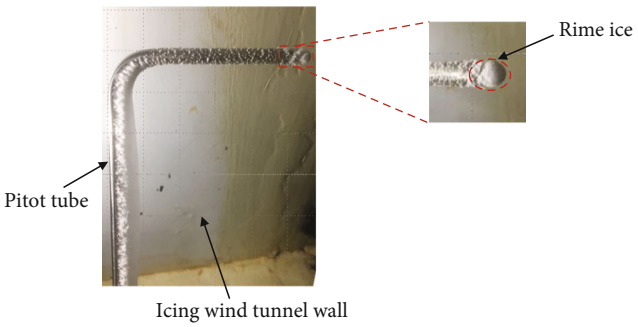

Figure 6: Pitot tube blocked by rime ice.

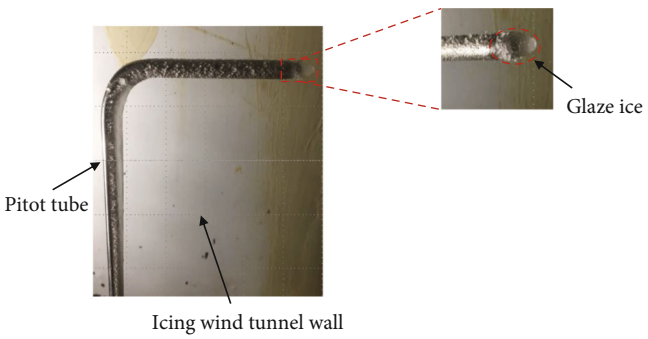

Figure 7: Pitot tube blocked by glaze ice.

groups D and E. Experiment D only opens the wind tunnel with the refrigeration and spray systems turned off. Experiment E opens the wind tunnel and spray system.

Table 5 presents the environmental parameters of experiment D. Figure 10 shows that when the pitot tube detection system is stationary, the total and static pressure outputs of the system are nearly the same, and the pressure difference is negligible. When the pitot tube is placed in the wind tunnel, the total pressure rises rapidly, whereas the static pressure slightly changes.

Table 6 indicates the parameters of experiment E. The spray system is turned on to simulate the state of water droplets under flight conditions. Figure 11 displays the experimental results of group E. The figure shows that when the pitot tube is placed in the ice wind tunnel after being static, the experimental results are similar to those of group A. At point B, the spray system is turned on, the water droplets come into contact with the pitot tube, the total pressure fluctuates, the spray system is turned off, and the total pressure returns to normal. The abovementioned experimental data

Figure 8: Rubber sleeve blocking the pitot tube.

Table 4: Experimental parameters of non-ice material blockage.

Experimental conditions	Temperature	Wind speed
Data	−5°C	18 m/s

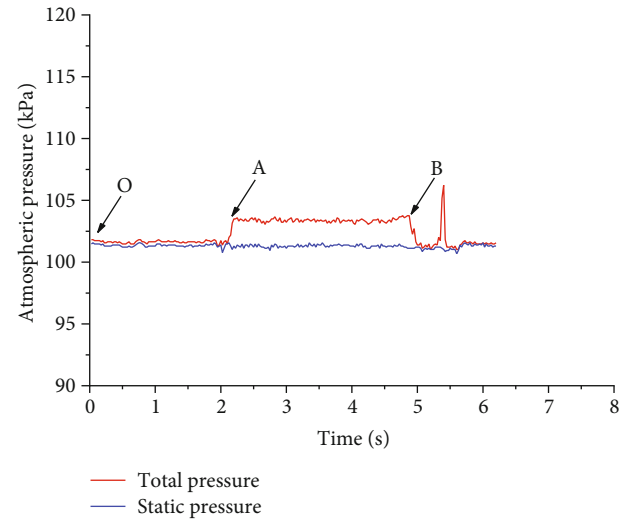

Figure 9: Total and static pressure outputs of the pitot tube after blocking by non-ice materials. O–A: the entire air pressure detection system is stationary. A–B: the L-shaped pitot tube is placed into the ice wind tunnel at point A such that the total pressure hole is facing the incoming wind direction. After B: the rubber sleeve is installed on the total pressure hole of the pitot tube at point B.

Table 5: Parameters of the normal temperature experiment.

Experimental condition	Temperature	Wind speed
Data	14.4°C	9.8 m/s

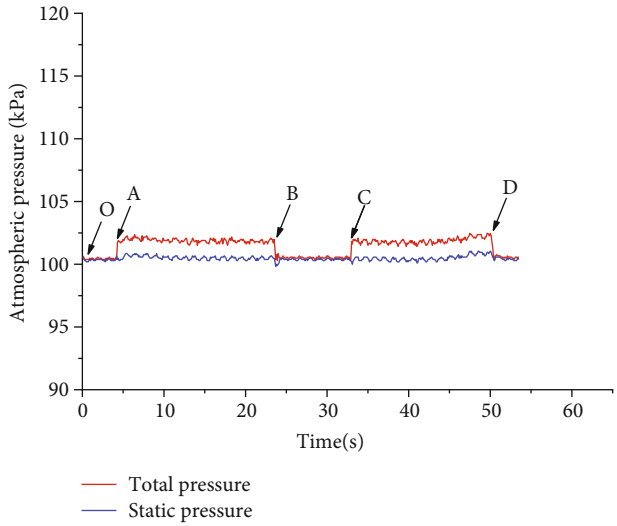

Figure 10: Total and static pressure outputs under normal temperature. O–A: the entire detection system is stationary. A-B: after the experimental environment reaches a stable state, the L-shaped pitot tube is placed into the ice wind tunnel at point A such that the total pressure hole is facing the incoming wind direction. After point B, the pitot tube is retracted at point B. C–D: the A–B operation is repeated.

Table 6: Experimental parameters for opening the spray system at normal temperature.

Experimental conditions	Mean volume diameter	Liquid water content	Temperature	Wind speed
Data	22 μm	0.715 g/m^3	14.4°C	9.8 m/s

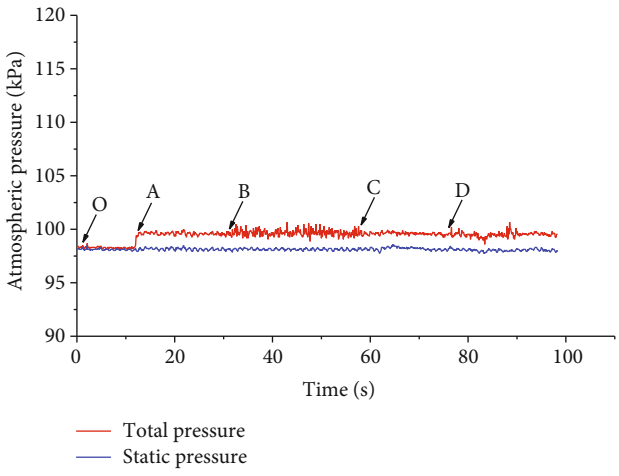

Figure 11: Total and static pressure outputs when the pitot tube is at normal temperature and the spray system is open. O–A: the entire air pressure detection system is stationary. A–B: the L-shaped pitot tube is placed into the ice wind tunnel at point A, and the total pressure hole is facing the incoming wind direction. B–C: the spray system is opened at point B to allow the water droplets to hit the pitot tube evenly. C–D: the spray system is closed at point C. After point D, the spray system is reopened.

indicate that after the pitot tube is placed in the ice wind tunnel, the total pressure immediately increases with the increase in wind speed. If the pitot tube comes into contact with water droplets but remains unfrozen, then the total pressure output value slightly fluctuates.

Repetitive experiments are conducted to ensure reliability. The parameters are changed to investigate the performance of the icing detection system at different conditions. The parameters are set as following values in this paper: MVD is 22 μm and 30 μm; LWC is 0.549 g/m^3 and 0.715 g/m^3; temperature is -5°C, -11.5°C, -10.4°C, 9°C, and 14.4°C; wind speed is 8.7 m/s, 7.9 m/s, 9.8 m/s, 11.4 m/s, 11 m/s, 12.3 m/s, 14.7 m/s, 15.6 m/s, and 18 m/s. Experiments are implemented based on the combination of some parameters. Details of more repetitive experiments are presented in the Supplementary Materials (available here).

4. Discussions

4.1. Ice Blocking Mechanism. Figure 12 illustrates the working mechanism of the pitot tube being blocked by rime ice. Rime ice is opaque and rough, and its structure ice is relatively loose [13]. A certain amount of air is present between ice crystal particles, such that its density and strength are low and enables air to flow through it. This factor creates the interface that further hinders airflow. When airflow enters the total pressure hole, multiple collisions occur with the obstructing interface, leading to energy loss and a decrease in dynamic pressure. Eventually, as the rime ice accumulates, the dynamic pressure P_q disappears, and the total pressure P_t becomes equal to static pressure P_s, as described in the following equation: $P_t = P_q + P_S = P_S$ (when $P_q = 0$). As a result, the total pressure gradually decreases and finally coincides with static pressure.

Figure 13 provides the working mechanism of the pitot tube being blocked by glaze ice. However, the accurate temperature of the front stage of the pitot tube is difficult to obtain due to equipment limitations. Therefore, only the trend of temperature change is shown. In the process of forming glaze ice, the temperature of the water droplets increases slightly due to the solidification of the water droplets such that the gas temperature at the front part of the pitot tube rises to the highest point T1 [14], and the total pressure hole is partially blocked. However, as ice accumulates and becomes increasingly thick, the heat released by solidification is not transmitted to the front end of the pitot tube and is dissipated by airflow. When temperature drops to T2, the total pressure hole of the pitot tube is completely blocked by glaze ice, which is smooth and transparent. As such, the structure becomes dense [13]. The slow icing speed makes the water droplets pile up closely together, and air bubbles are eliminated in a relatively thorough manner such that a confined space is formed inside the pitot tube. The temperature continues to drop, which can be explained by the ideal gas equation (Eq. (1)). The variables v, n, and R are unchanged because the cavity is sealed, whereas P decreases with the decrease in T. However, when T is the same as ambient temperature, P no longer falls to reach stability. As a result, the

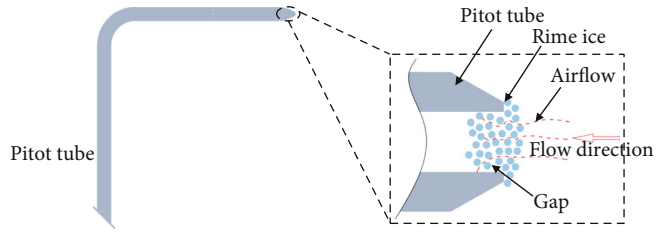

Figure 12: Rime ice blocking the total pressure hole of the pitot tube.

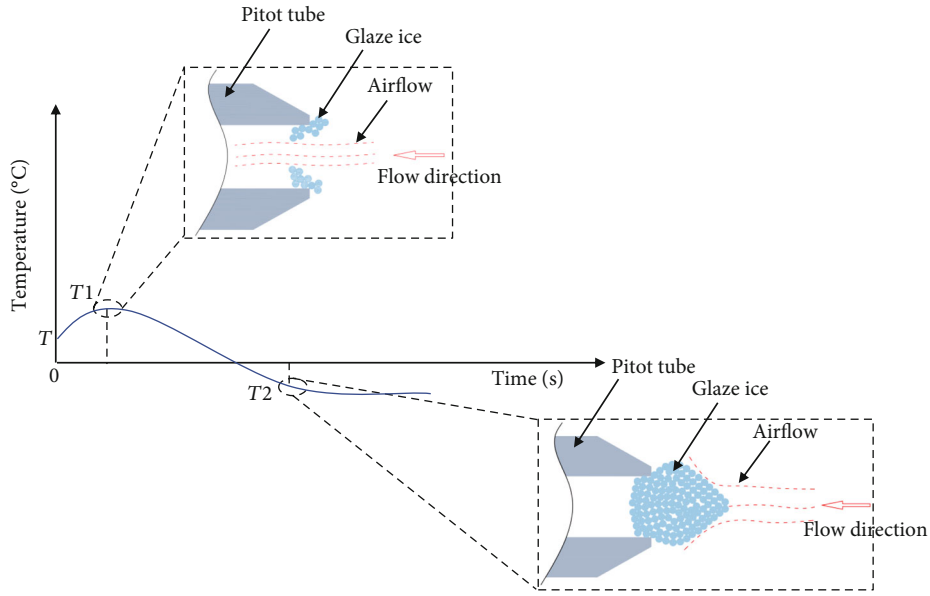

Figure 13: Temperature change of the pitot tube blocked by glaze ice. At the beginning of the experiment, the initial temperature of the pitot tube is assumed to be T. After the water droplets solidified for a period, the pitot tube temperature reaches $T1$. At this time, the pitot tube is partially blocked, and the temperature of the pitot tube drops. At $T2$, the pitot tube is completely blocked.

total pressure decreases gradually to a value less than the static pressure and then stabilizes.

$$PV = nRT, \tag{1}$$

where P is the pressure of ideal gas, V is the volume of the ideal gas, n is the amount of gaseous matter, T is thermodynamic temperature of ideal gas, and R is ideal gas constant.

4.2. Non-Ice Organic Material Blocking Mechanism. Dynamic pressure increases under the action of wind speed such that the total pressure of the pitot tube increases. When the pitot tube is blocked by the rubber sleeve, a portion of the gas inside the rubber sleeve is compressed into the total pressure tube, and the total pressure suddenly increases. The total pressure hole cannot detect the dynamic pressure under the action of the rubber sleeve; thus, dynamic pressure is reduced to zero, whereas the total pressure becomes consistent with the static pressure. When the rubber sleeve is removed, a portion of the gas inside the pitot tube is released, causing a sudden drop in the total pressure.

It can be inferred that the total pressure will only immediately decrease to the static pressure value without abrupt rise when the pitot tube is blocked by the insect, since the insect is different from the rubber sleeve.

The difference between the rubber sleeve and insect is further discussed here. In this paper, the rubber sleeve is used because the insect itself is an organic substance, and the rubber sleeve is also an organic substance. At the same time, neither of these two substances is a heating source and does not generate heat. Thus, the rubber sleeve could be used as an alternative for insect. However, because the rubber sleeve is a columnar structure, there will be some air inside it. When the pitot tube is blocked with a rubber sleeve, the air will be compressed into the pitot tube cavity, resulting in a brief rise in the total pressure. While for insect clogging, no such a brief rise in the total pressure since there is no big cavity inside the insect, and thus no air compressed into the pitot tube.

4.3. Water Spray Mechanism. The pitot tube is statically placed in the atmosphere. When placed in the ice wind tunnel and under the action of wind speed, dynamic pressure $P_q = 1/2\rho v^2$ increases. Therefore, the total pitot tube pressure $P_t = P_q + P_s$ also increases and is denoted as point A in Figure 10 and shown as the red line with a rapid increase.

When the spray system is turned on, the flow of the wind tunnel changes under the influence of the gas path of the spray system, and liquid droplets hit the total pressure hole

of the pitot tube. As a result, the total pressure fluctuation is detected by the pitot tube.

4.4. Data Analysis of Icing Detection. The pitot tube icing detection system could detect the ice accretion through the variation of pressure based on the analysis of collected pressure data. The analysis process and the determined standard are discussed as follows. Take the static pressure Y_s as a fixed value, and take the total pressure as Y_t, Y_{t+k}, $Y_{t+2k} \cdots \cdots Y_{t+ik}$. Let $A1 = Y_{t+k} - Y_t$, $A2 = Y_{t+2k} - Y_t$, $A3 = Y_{t+3k} - Y_t \ldots$ $\ldots Ai = Y_{t+ik} - Y_t$; If $(1/n+1)\sum_{i=0}^{n} Y_{t+ik} \gg Y_s$ and $(1/n)\sum_{i=1}^{n} A_i < W_1$kPa, it is the stable fly stage (e.g., the A-B segment of pressure output as shown in Figure 4); If $(1/n+1)\sum_{i=0}^{n} Y_{t+ik} \gg Y_s$ and $W_1 < (1/n)\sum_{i=1}^{n} A_i < W_2$kPa, it is the water droplets impacting stage (e.g., the B-C segment of pressure output as shown in Figure 4); If $(1/n+1)\sum_{i=0}^{n} Y_{t+ik} > Y_s$ and $|A1|, |A2|, |A3| \cdots \cdots |Ai|$ are gradually increasing, it is the ice accretion stage (e.g., the C-D segment of pressure output as shown in Figure 4); If $(1/n+1)\sum_{i=0}^{n} Y_{t+ik} = Y_s$ and $(1/n)\sum_{i=1}^{n} A_i < W_1$kPa, it is rime ice stage (e.g., the segment after point D of pressure output as shown in Figure 4); If $(1/n+1)\sum_{i=0}^{n} Y_{t+ik} < Y_s$ and $(1/n)\sum_{i=1}^{n} A_i < W_1$kPa, it is glaze ice stage (e.g., the segment after point D of pressure output as shown in Figure 6). Where k is the time interval which depends on the sampling frequency and preset accuracy; i is the number of samples; and W_1 and W_2 are the judgment thresholds, which depend on experimental results and preset accuracy, and could be obtained after analyzing a large amount of experimental data at different conditions.

The detection system can only judge if there is ice or not, and further what kind of ice it is. However, the system is currently unable to detect the icing thickness and ice accretion rate in time. Therefore, it is hard to discuss the sensitivity of the system if the sensitivity here is defined as the ratio of the pressure to the icing thickness. To detect icing thickness and ice accretion rate in time, more details about the ice accretion process should be further studied with better experimental conditions. The good news is that telling yes or no of ice is acceptable for small and medium UAV applications since they do not have any icing measurement equipment now.

4.5. Effect on Flight Safety. The traditional pitot tube is installed at the leading edge of the aircraft nose to indicate the current airspeed of the aircraft. If it is blocked by ice, it will have a potential impact on flight safety due to the wrong airspeed information. However, the pitot tube icing detection system does not pose a safety hazard to the aircraft.

The pitot tube-based icing detection system and airspeed detection system are two separate systems. Another pitot tube instead of the airspeed detecting one is used in the icing detection system. It is installed on the leading edge of the wing instead of the nose. The pressure data obtained of the pitot tube fixed in the wing is only used for icing detection but not for airspeed detection. The aerodynamic analysis should be implemented to make sure that the extruding part of the pitot tube-based ice detection system, even with ice accretion, will have minimum effect on its aerodynamic performance, like extruding parts of other aircraft instruments. Therefore, the pitot tube-based icing detection system will not affect the flight safety.

The UAVs will take some actions when the icing detection system alarm, for example, fly out of the icing zone, to prevent the icing hazard. The pitot tube in the icing detection system will be blocked by ice when the system detects icing. Then the ice on the pitot tube will be removed by heating so that the system can work again when it faces ice in the future.

5. Conclusions

In this study, an icing detection method based on the pitot tube is proposed. A corresponding icing detection system based on the pitot tube is designed and fabricated. Experiments using ice, non-ice organic materials, and water are conducted in the icing wind tunnel. The traditional understanding is that the output value will change after the pitot tube is blocked, but the law of its change is not clear. This article obtains the semiquantitative law of the pitot tube blocked by rime ice, glaze ice, non-ice organic materials, and water droplets. Results show that after the pitot tube is blocked by ice, the total pore output characteristics of the pitot tube declines, whereas static pressure remains basically unchanged. When the icing state is rime ice, the total pressure drops to the level of the static pressure and remains unchanged. When the icing state is glaze ice, the total pressure continues to decrease and reaches a level lower than the static pressure and remains unchanged. If non-ice organic materials block the pitot tube, then the total pressure output characteristic is a cutoff signal and does not indicate a slow process, which is remarkably different from the blockage of icing material. If the pitot tube comes into contact with water droplets but are unfrozen, then the total pressure output value fluctuates slightly. This facile and low-cost icing detection method based on the pitot tube has great potential for UAV safety.

Data Availability

The TXT data used to support the findings of this study are available from the corresponding author upon request.

Conflicts of Interest

The authors declare that there is no conflict of interest regarding the publication of this paper.

Acknowledgments

The research work is partially supported by the National Natural Science Foundation of China (Grant Nos. 51875478 and 51735011), the Aeronautical Science Foundation of China (Grant No. 2017ZC53036), the Special Scientific Research Project (MJ-2016-F-07), and the 111 Project (Grant No. B13044).

Supplementary Materials

In this section, repeated experiments are provided, see Figures 1–10 in the supplementary material. *(Supplementary Materials)*

References

[1] J. S. Visockiene, R. Puziene, A. Stanionis, and E. Tumeliene, "Unmanned aerial vehicles for photogrammetry: analysis of orthophoto images over the territory of Lithuania," *International Journal of Aerospace Engineering*, vol. 2016, 9 pages, 2016.

[2] A. Reehorst, J. Chung, M. Potapczuk, and Y. Choo, "Study of icing effects on performance and controllability of an accident aircraft," *Journal of Aircraft*, vol. 37, no. 2, pp. 253–259, 2000.

[3] W. A. Cooper, W. R. Sand, M. K. Politovich, and D. L. Veal, "Effects of icing on performance of a research airplane," *Journal of Aircraft*, vol. 21, no. 9, pp. 708–715, 1984.

[4] W. R. Sand, W. A. Cooper, M. K. Politovich, and D. L. Veal, "Icing conditions encountered by a research aircraft," *Journal of Applied Meteorology*, vol. 23, no. 10, pp. 1427–1440, 1984.

[5] C. Zilio and L. Patricelli, "Aircraft anti-ice system: evaluation of system performance with a new time dependent mathematical model," *Applied Thermal Engineering*, vol. 63, no. 1, pp. 40–51, 2014.

[6] F. Zhang, W. Deng, H. Nan, L. Zhang, and Z. Huang, "Reliability analysis of bleed air anti-icing system based on subset simulation method," *Applied Thermal Engineering*, vol. 115, pp. 17–21, 2017.

[7] F. Zhang, Y. Gao, H. Yao, Y. Wang, and K. Luo, "Structural parameter sensitivity analysis of an aircraft anti-icing cavity based on thermal efficiency," *International Journal of Aerospace Engineering*, vol. 2019, 7 pages, 2019.

[8] A. A. Ikiades, D. J. Armstrong, G. G. Hare, M. Konstantaki, and S. D. Crossley, "Fiber optic sensor technology for air conformal ice detection," in *Proceedings of SPIE-The International Society for Optical Engineering*, 2004.

[9] X. Zhi, H. Cho, B. Wang, C. Ahn, H. Moon, and J. Go, "Development of a capacitive ice sensor to measure ice growth in real time," *Sensors*, vol. 15, no. 3, pp. 6688–6698, 2015.

[10] S. Roy, R. G. DeAnna, A. Izad, and M. Mehregany, "Miniature ice detection sensor systems for aerospace applications," in *Proceedings MEMS 98. IEEE. Eleventh Annual International Workshop on Micro Electro Mechanical Systems. An Investigation of Micro Structures, Sensors, Actuators, Machines and Systems (Cat. No.98CH36176)*, Heidelberg, Germany, Germany, Jan 1998.

[11] P. Jarvinen, "Detection of pitot-static icing at high altitudes," in *51st AIAA Aerospace Sciences Meeting including the New Horizons Forum and Aerospace Exposition*, Grapevine (Dallas/Ft. Worth Region), Texas, January 2013.

[12] R. Klopfenstein Jr., "Air velocity and flow measurement using a pitot tube," *ISA Transactions*, vol. 37, no. 4, pp. 257–263, 1998.

[13] R. J. Kind, M. G. Potapczuk, A. Feo, C. Golia, and A. D. Shah, "Experimental and computational simulation of in-flight icing phenomena," *Progress in Aerospace Sciences*, vol. 34, no. 5-6, pp. 257–345, 1998.

[14] Z. Mu, G. Lin, X. Shen, X. Bu, and Y. Zhou, "Numerical simulation of unsteady conjugate heat transfer of electrothermal deicing process," *International Journal of Aerospace Engineering*, vol. 2018, 16 pages, 2018.